PAPER

Quantum dynamics simulations: combining path integral nuclear dynamics and real-time TDDFT

View the article online for updates and enhancements.

Electronic Structure

PAPER

Quantum dynamics simulations: combining path integral nuclear dynamics and real-time TDDFT

Peiwei You[1,3], Jiyu Xu[1,3] ⓘ, Chao Lian[1], Cui Zhang[1], Xin-Zheng Li[4,5], En-Ge Wang[1,2,4,5] and Sheng Meng[1,2,3,5] ⓘ

1 Beijing National Laboratory for Condensed Matter Physics and Institute of Physics, Chinese Academy of Sciences, Beijing 100190, People's Republic of China
2 Songshan Lake Materials Laboratory, Dongguan, Guangdong 523808, People's Republic of China
3 School of Physical Sciences, University of Chinese Academy of Sciences, Beijing 100049, People's Republic of China
4 State Key Laboratory for Artificial Microstructure and Mesoscopic Physics and School of Physics, Peking University, Beijing 100871, People's Republic of China
5 Collaborative Innovation Center of Quantum Matter, Beijing 100190, People's Republic of China

E-mail: smeng@iphy.ac.cn

Abstract

We report a practical computational scheme for quantum electron-nuclear dynamic simulations, applicable to both finite (e.g. ozone) and periodic systems (e.g. graphene), using a combination of real-time time dependent density functional theory (rt-TDDFT) and ring polymer molecular dynamics. This scheme could deal with quantum effects of nuclei beyond Ehrenfest dynamics in TDDFT simulations. We find that when nuclear quantum effects (NQEs) are taken into account, the atomic structure of ozone splits into normal states and cyclic states upon photoexcitation. NQEs broaden the electronic density of states and induce strong orbital couplings, leading to new nuclear trajectories and carrier dynamics different from classical simulations. We also observe a charge carrier redistribution accelerated by the quantum motions of carbon atoms in graphene, yielding an exponential decay with fast relaxation time. These developments and practices represent an advance in studying full quantum dynamics of electrons and nuclei from first-principles, towards a complete and predictive understanding of quantum interactions and dynamics in large molecules and complex materials at the microscopic level.

Exact or numerical solution of the time dependent Schrödinger equation (TDSE) in the presence of external field is a major challenge for modern computer simulations of materials. However, many nonadiabatic phenomena such as chemical reactions [1–3], electron-phonon couplings [4, 5] and ultrafast dynamics [6–8] require a quantum treatment of many-body TDSE in practical simulations. Some *ab initio* quantum dynamic simulations have been carried out in the past [9–18]. Full quantum dynamics such as multi-configuration time-dependent Hartree [9, 10] (MCTDH) can provide exact results for small molecules, but MCTDH is restricted by the number of nuclear degrees of freedom that can be explicitly accounted for in the method, preventing its efficient use for large molecules and complex materials. An advanced method, variational multiconfigurational Gaussian wave packet method [18], offers a way to solve on-the-fly the time-dependent molecular Schrödinger equation, including all quantum nuclear effects, and has been coupled with *ab initio* electronic structure methods. Another popular approach, multiple spawning [11], can converge to exact solutions for small systems but is limited by the truncation of large basis set. Involving classical nuclear approximations, fewest-switches surface-hopping algorithm [12, 13] (FSSH) and Ehrenfest dynamics [14–17] are the dominating simple approaches feasible for large-scale mixed quantum–classical dynamics simulations of realistic materials at the present.

To treat the quantum property of nuclei, ring polymer molecular dynamics (RPMD) based on imaginary-time path integral simulations of nuclear trajectory has been introduced [19, 20]. Recently, Tully *et al* has made a breakthrough developing the nonadiabatic dynamics simulation method of RPMD implemented with FSSH, to incorporate proper treatment of quantum nuclear behaviors in nonadiabatic surface hopping simulations

[21]. Nevertheless, the heavy computational costs limit most FSSH simulations working with either an empirical model Hamiltonian or only a ground-state potential energy surface (PES) in practice. On the other hand, Ehrenfest dynamics as a mean-field theory has been widely used in real time simulations of nonadiabatic electron-nuclear motions. Previous works have combined RPMD with Ehrenfest dynamics using one-electron TDSE and empirical potentials to study electron-nuclear dynamics of a single silver-atom embedded in helium clusters and water anion clusters, but they are strictly constrained to these model systems [22–25]. A widely used approach to treat quantum nuclear effects in nonadiabatic molecular dynamics simulations fully based on first principles is still missing.

Here we present a new strategy for simulating electron-nuclear quantum motions by implementing RPMD in the frame of first principles real-time time dependent density functional theory (rt-TDDFT). Although it follows the factorization of the total wavefunction into dependent electronic part and nuclear part, this method goes beyond the popular Ehrenfest scheme, because the classical limitations on the nuclei trajectory are lifted. As prototype examples to demonstrate its feasibility, the approach has been successfully applied to both finite (e.g. ozone) and extended systems (e.g. graphene) to demonstrate the quantum electronic and nuclear dynamics upon photoexcitation. Different from classical dynamic simulations, quantum wave packet of ozone splits into normal states and cyclic states during the evolution of electronically excited states. The distinction between quantum and classical treatments for the nuclear motions in extended system is also shown. Quantum electron-nuclear dynamics in graphene exhibits an exponential carrier relaxation process, where the redistribution of charge carriers in energy is faster than that in classical-nuclei simulations, confirming the importance of quantum behaviors of nuclei in ultrafast electronic dynamics in condensed matters.

Methodology

Starting from TDSE, the Hamiltonian of a combined electronic and nuclear system is

$$\widehat{H}_{\text{tot}}\left(\mathbf{r}, \mathbf{R}, t\right) = \widehat{T}_{\text{N}}(\mathbf{R}) + \widehat{H}_{\text{BO}}\left(\mathbf{r}, \mathbf{R}\right) + U_{\text{ext}}\left(\mathbf{r}, \mathbf{R}, t\right) \tag{1}$$

where $\mathbf{r}$ and $\mathbf{R}$ denote the collective coordinates of electronic positions $\mathbf{r}_i$ and nuclear positions $\mathbf{R}_\alpha$. $\widehat{T}_{\text{N}}$ represents the nuclear kinetic energy part, and U_{ext} is the external potential. While $\widehat{H}_{\text{BO}}$ is the electronic Hamiltonian given by

$$\widehat{H}_{\text{BO}}\left(\mathbf{r}, \mathbf{R}\right) = \sum_i \frac{p_i^2}{2m} + \sum_{i<j} \frac{e^2}{|\mathbf{r}_i - \mathbf{r}_j|} - \sum_{i,\alpha} \frac{eZ_\alpha}{|\mathbf{r}_i - \mathbf{R}_\alpha|} + \sum_{\alpha,\beta} \frac{Z_\alpha Z_\beta}{|\mathbf{R}_\alpha - \mathbf{R}_\beta|}$$
$$= \widehat{T}_{\text{el}} + V\left(\mathbf{r}, \mathbf{R}\right). \tag{2}$$

Here m is the mass of electrons and Z_α is the ionic charge; $\widehat{T}_{\text{el}}$ is the electronic kinetic energy and the rest part is denoted as $V\left(\mathbf{r}, \mathbf{R}\right)$. Based on factorization of the total wavefunction into the product of electron and nuclei parts, the time-dependent self-consistent field formula (TDSCF) is derived [14, 16]. In this simplification, the entanglement between electronic and nuclear degrees of freedom is lost, and therefore the Berry phase of electronic wavefunction with respect to nuclear coordinates under the derivation disappears [26, 27]. Without the classical-nuclei approximation, we obtain TDSCF equations with the external field:

$$i\hbar \frac{\partial}{\partial t} \varphi\left(\mathbf{r}, t\right) = \left[\widehat{T}_{\text{el}} + \int d\mathbf{R} \chi^*\left(\mathbf{R}, t\right) \left[V\left(\mathbf{r}, \mathbf{R}\right) + U_{\text{ext}}\left(\mathbf{r}, \mathbf{R}, t\right)\right] \chi\left(\mathbf{R}, t\right)\right] \varphi\left(\mathbf{r}, t\right) \tag{3}$$

$$i\hbar \frac{\partial}{\partial t} \chi\left(\mathbf{R}, t\right) = \left[\widehat{T}_{\text{N}} + \int d\mathbf{r} \varphi^*\left(\mathbf{r}, t\right) \left[\widehat{H}_{\text{BO}}\left(\mathbf{r}, \mathbf{R}\right) + U_{\text{ext}}\left(\mathbf{r}, \mathbf{R}, t\right)\right] \varphi\left(\mathbf{r}, t\right)\right] \chi\left(\mathbf{R}, t\right) \tag{4}$$

where $\varphi\left(\mathbf{r}, t\right)$ is electronic wavefunction and $\chi\left(\mathbf{R}, t\right)$ represents nuclear wavefunction. Different from normal TDSCF, the external field is introduced and the new electronic Hamiltonian can be defined as $\widehat{H}_{\text{eff}}\left(\mathbf{r}, \mathbf{R}, t\right) = \widehat{H}_{\text{BO}}\left(\mathbf{r}, \mathbf{R}\right) + U_{\text{ext}}\left(\mathbf{r}, \mathbf{R}, t\right)$. The nuclear motion is evolved in a mean field of electronic states. We define the mean field as:

$$U\left(\mathbf{R}, t\right) \equiv \int d\mathbf{r} \varphi^*\left(\mathbf{r}, t\right) \widehat{H}_{\text{eff}}\left(\mathbf{r}, \mathbf{R}, t\right) \varphi\left(\mathbf{r}, t\right). \tag{5}$$

At each time, the mean field acting on nuclear motion is calculated in the first-principles framework using time-dependent density functional theory.

Next, the nuclear self-consistent field in equation (4) is calculated using RPMD with the nuclear Hamiltonian expressed in the path integral approach:

$$H_n\left(\mathbf{p}, \mathbf{R}, t\right) = \sum_{j=1}^{n} \left[\frac{|\mathbf{p}_j|^2}{2M} + \frac{1}{2} M\omega_n^2 |\mathbf{R}_j - \mathbf{R}_{j-1}|^2\right] + \sum_{j=1}^{n} U_j\left(\mathbf{R}, t\right) \tag{6}$$

where $H_n(\mathbf{p}, \mathbf{R})$ is the Hamiltonian of n-bead ring polymers with the potential $U(\mathbf{R}, t)$ related to electronic states. Here M is the mass of nuclei and ω_n is the frequency of the spring connecting n-bead ring polymers. Then we perform RPMD simulations to obtain the evolution of nuclear coordinates generated by the Hamiltonian $H_n(\mathbf{p}, \mathbf{R}, t)$:

$$\dot{\mathbf{p}}_j = -\frac{\partial H_n(\mathbf{p}, \mathbf{R}, t)}{\partial \mathbf{R}_j} \tag{7}$$

$$\dot{\mathbf{R}}_j = \frac{\partial H_n(\mathbf{p}, \mathbf{R}, t)}{\partial \mathbf{p}_j}. \tag{8}$$

The principles of RPMD assure quantum statistics and semi-classical dynamics of the system using ring polymers [19]. Since each bead is recognized as comprising classical nuclei, we apply

$$\chi_j(\mathbf{R}, t) \rightarrow \sum_{\alpha} \delta(\mathbf{R}(t) - \mathbf{R}_{\alpha}(t)) \tag{9}$$

to the right side integral in equation (3). The integral is vanished by delta function and we can then use $\left[\hat{T}_{el} + V(\mathbf{r}, \mathbf{R}) + U_{ext}(\mathbf{r}, \mathbf{R}, t)\right] \equiv \hat{H}_{eff}(\mathbf{r}, \mathbf{R}, t)$. In this approach, the nuclear wavefunction $\chi(\mathbf{R}, t)$ is thus sampled by a sufficient number of classical beads, connected by the strings whose elastic constant is proportional to the temperature, in the same way as regular RPMD does.

The electronic wavefunction equation (3) is degraded into rt-TDDFT equation for each bead:

$$i\hbar \frac{\partial}{\partial t} \varphi_j(\mathbf{r}, t, \mathbf{R_t}) = \hat{H}_{eff}^j(\mathbf{r}, \mathbf{R_t}, t) \varphi_j(\mathbf{r}, t, \mathbf{R_t}). \tag{10}$$
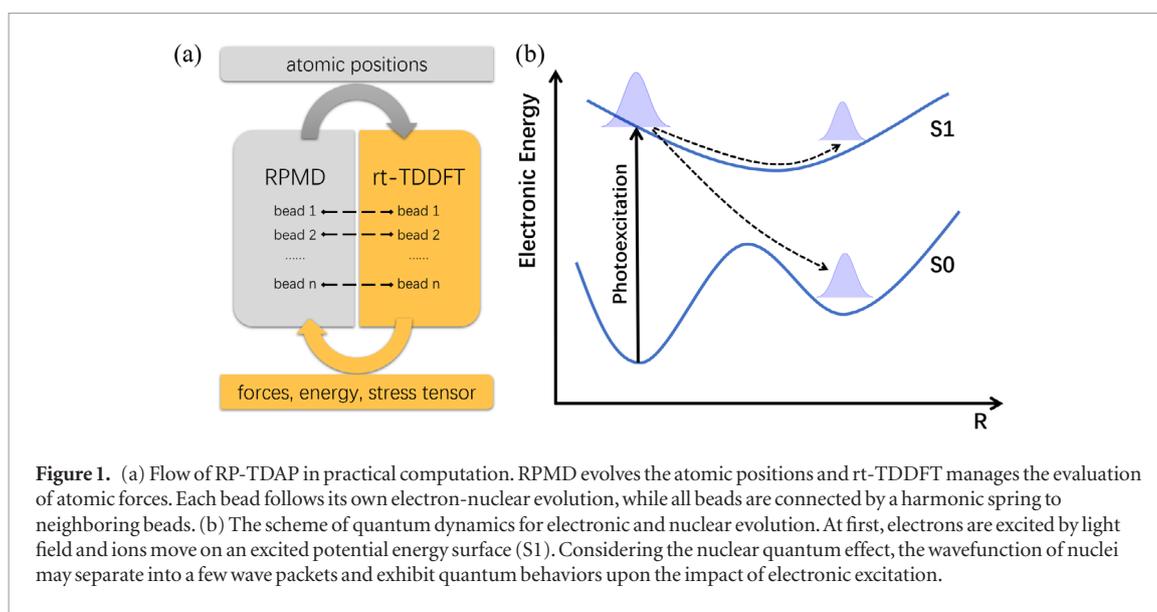
Neighboring beads of the same atom interact through spring interactions. We define this approximation as first-order approximation in the quantum limit. In practical simulations, RPMD requires a finite number of classical beads to do the path integral. In this regard, approximations in equations (3) and (4) are actually the same; both apply classical limits for each bead. One can extract the quantum distribution of atoms in the position space due to the presence of quantum zero point motions in the mean-field potential, which are fully included statistically in RPMD simulations. Overall, if information on all beads is collected, the two equations present a certain extent of quantum nuclear effects to both nuclei evolution and electronic propagation. The principles of RPMD are used to arrive to this level of approximation naturally. In principle, a new electronic equation accounting for the quantum description of the nuclei can also be used, however, it would be confronted with the classical trajectory for each bead and the final superposed state is hard to interpret. We also notice that in Tully's RPSH scheme, it is assumed that all of the beads of a ring polymer reside *on a single electronic state* at all times, except for instantaneous hops. The consistency between nuclear forces and electronic states of each bead is maintained. In our approach, we also keep this consistency between nuclear forces and electronic states for each bead, namely, each bead is required to follow the nuclear trajectory determined by the bead's electronic states.

In summary, electronic evolution is calculated by equation (10) and the nuclear trajectory is dealt with RPMD evolution using equations (7) and (8). The external potential in RPMD is given by the dynamical electronic calculations based on rt-TDDFT. Full computational flow is shown in figure 1(a). In practical calculations, the data obtained from rt-TDDFT contains ionic forces, electronic energy and stress tensor, while RPMD manages the evolution of atomic positions and velocities [28, 29]. Since all of these are time-evolving and each bead must follow the constraints from last steps, we modify the parallel strategy to satisfy this need. For convenience, we name this approach as ring polymer time-dependent *ab initio* propagation (RP-TDAP) method, as schematically shown in figure 1(b).

Results

Ozone

We first apply the above developed approach to a simple molecule, ozone, to show the quantum splitting of nuclear motions when considering the nuclear quantum effects. Ozone, existing in the atmosphere and screening the earth from ultraviolet solar radiation, has been intensively studied from both experimental [30–32] and theoretical [33–41] aspects. Here we focus on the quantum dynamics of excited states in ozone under a strong laser field. The total energy, bond angle and oxygen–oxygen distances of the ozone molecule are calculated with 4, 8, 12 and 16 beads, respectively, to check the convergence in RPMD simulations, as shown in figure S1 (stacks. iop.org/EST/1/044005/mmedia). The distribution of ozone bond angles and oxygen–oxygen bond lengths are found to be stabilized with employing 12 beads. Therefore, we first perform path-integral molecular dynamics simulations of ozone with 12 beads in the canonical (NVT) ensemble at 20, 300, 1000 K, respectively, where the molecule is equilibrated for 2 ps. Then an ultraviolet light with a photon energy of 8.75 eV is applied to irradiate ozone via the RP-TDAP approach, under the micro-canonical (NVE) ensemble. As shown in figure 2(a), the light

Figure 1. (a) Flow of RP-TDAP in practical computation. RPMD evolves the atomic positions and rt-TDDFT manages the evaluation of atomic forces. Each bead follows its own electron-nuclear evolution, while all beads are connected by a harmonic spring to neighboring beads. (b) The scheme of quantum dynamics for electronic and nuclear evolution. At first, electrons are excited by light field and ions move on an excited potential energy surface (S1). Considering the nuclear quantum effect, the wavefunction of nuclei may separate into a few wave packets and exhibit quantum behaviors upon the impact of electronic excitation.

intensity is 0.25 V Å^{-1} with a full width at half maximum (FWHM) of 12 fs, polarized along the y axis parallel to the direction of large transition dipole moment in the ozone molecule [40].

We first compare the radius of gyration at different temperatures, which is calculated by the root mean square distance from bead to centroid, in figure 2(b). The radius represents the spatial spreading of the quantum wave packets of nuclei. As shown in figure 2(b), the radius grows in an inverse proportion to the square root of temperature, which indicates more significant quantum effects at low temperatures. The time evolutions of oxygen–oxygen (O–O) distances in ozone molecule at 20, 300, and 1000 K are shown in figures 2(c)–(e), respectively. The solid lines represent the distances between oxygen centroids, and the corresponding shadows demonstrate the spread of distances between oxygen beads, mainly caused by the quantum fluctuations. Photo-excitation process results in shortened oxygen distances in ozone molecule, especially for the distance between two ending oxygens (O$_2$–O$_3$). At 300 and 1000 K, the ozone structure varies from isosceles to equilateral configurations after photoexcitation. In comparison, at 20 K the distances between oxygen centroids in ozone decrease but remain the initial equilateral configuration, with significantly larger spreading. The remarkable broadening of oxygen distance spreading (shadows) not only indicates the pronounced quantum effects at low temperature, but also suggests mixed structure configurations yielded upon laser excitation.

We further investigate the quantum structure and dynamics of photoexcited ozone molecule at 20 K. Previous quantum chemistry studies pointed out that ozone has two local minima structures, the normal ground state form and the cyclic form, separated by ~1.3 eV in energy [41]. We then separate the beads at 70 fs into normal and cyclic states based on a geometrical criterion, as shown in figure 3(a): beads with O–O bond lengths between 1.2–1.3 Å and an angle around 120° are defined as normal states, while those in equilateral configuration with a O–O distance of ~1.0 Å are distinguished as the cyclic state. We compare the number of excited electrons and oxygen distances of two types of beads in figures 3(b) and (c), respectively. It shows that the beads with higher population of excited electrons begin to evolve into the cyclic state starting from 20 fs, right after the peak time of laser field. Consequently, the equilateral cyclic structures are formed at ~70 fs. We also analyze the radius of gyration for the beads in the normal and cyclic states, as shown in figure 4. During the whole photo-excitation process studied, the radius of gyration for the beads in the normal state remains nearly constant, representing a localized wave packet close to the centroid. In contrast, the radius of gyration for the beads in the cyclic configuration starts to increase after absorbing light, indicating the formation of delocalized wave packets spreading away from the centroid. It is also noticed that these transient cyclic states forms a shorter bond length of ~1.0 Å (see figure 3(c)) than that in equilibrium cyclic configuration (1.45 Å [41]), which is attributed to the high energy excitation.

The evolution of photo-induced electronic structures of the two typical configurations, the normal and cycle states, are presented in figure S2. The electron population in the excited states of beads in the cyclic state can be nearly five times larger than that in the normal state (also see figure 3(b)). It is obvious that the electronic density of states is broadened when considering NQEs, attributed to the random quantum fluctuations in atomic configurations away from the equilibrium one (figure S3). Photogenerated electrons in ozone molecule by an 8.75 eV laser pulse are expected to experience an electronic transition from the second highest occupied molecular orbital (HOMO-1) to the second lowest unoccupied molecular orbital (LUMO + 1) (see figures S2(c) and (d)). Distinct fluctuations in the electronic energy levels of the beads in the cyclic state indicate stronger couplings between the HOMO-1 and LUMO + 1 orbitals, as compared to the other beads.
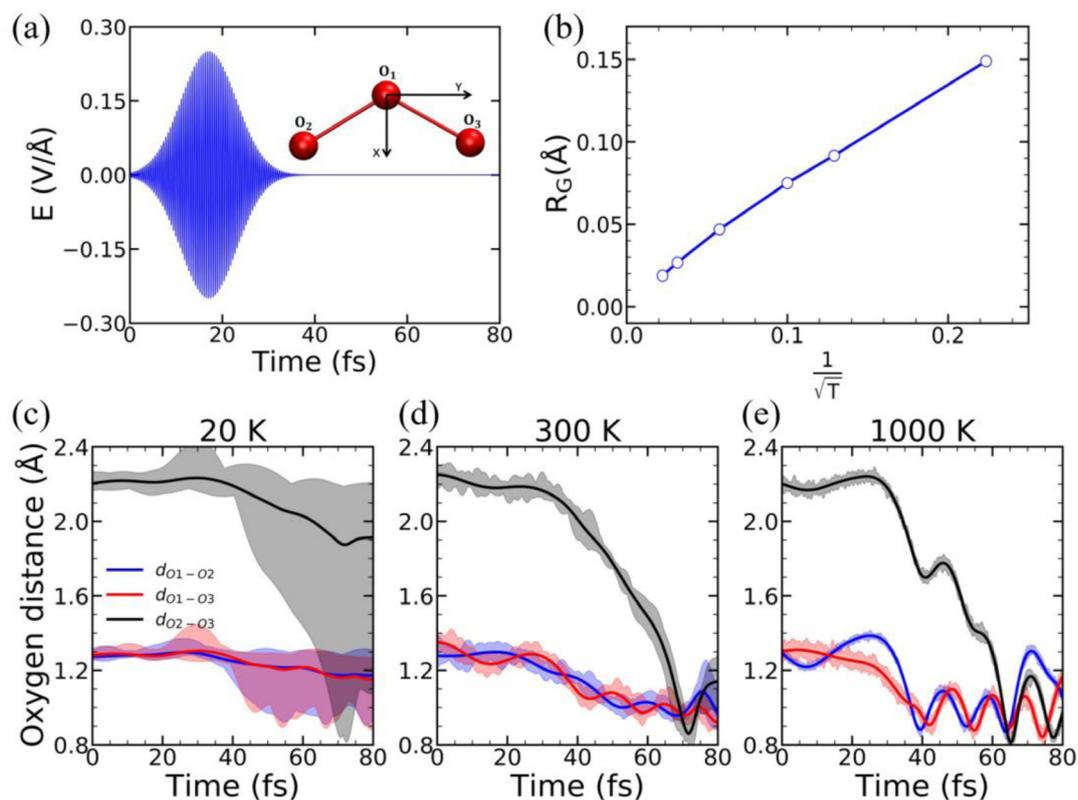
Figure 2. (a) Time-dependent waveform of the laser field with a photon energy of 8.75 eV and a field strength of 0.25 V Å⁻¹. The polarization direction is along the *y* axis, the direction jointing two ending oxygen atoms in ozone molecule. (b) The radius of gyration as a function of temperature. The radius, representing the quantum wave packet of nuclei, is inversely proportional to the square root of temperature. Figures (c)–(e) are the time evolutions of oxygen distances in the ozone molecule at 20, 300, and 1000 K, respectively, under ultraviolet illumination. The solid lines describe the distances between the oxygen centroids and the corresponding shadows display the effects of spatial spreading of quantum beads.
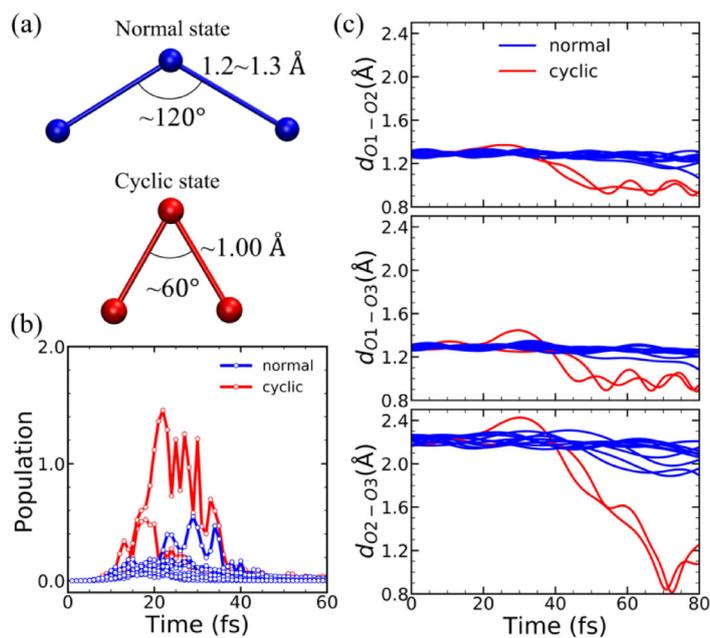

Figure 3. (a) Atomic configurations of ozone in the normal and cyclic states. (b) The number of excited electrons in each bead of ozone molecule as a function of time at 20 K. (c) Temporal distance of three oxygen atoms in each bead at 20 K. We separate all beads into normal (blue) and cyclic states (red), according to a geometrical criterion (see text).
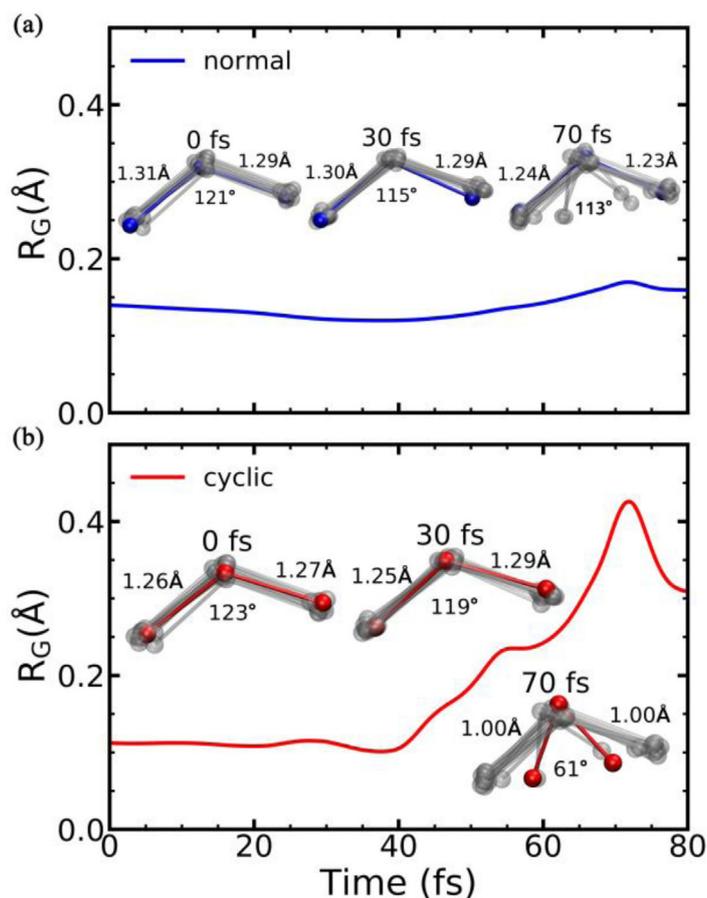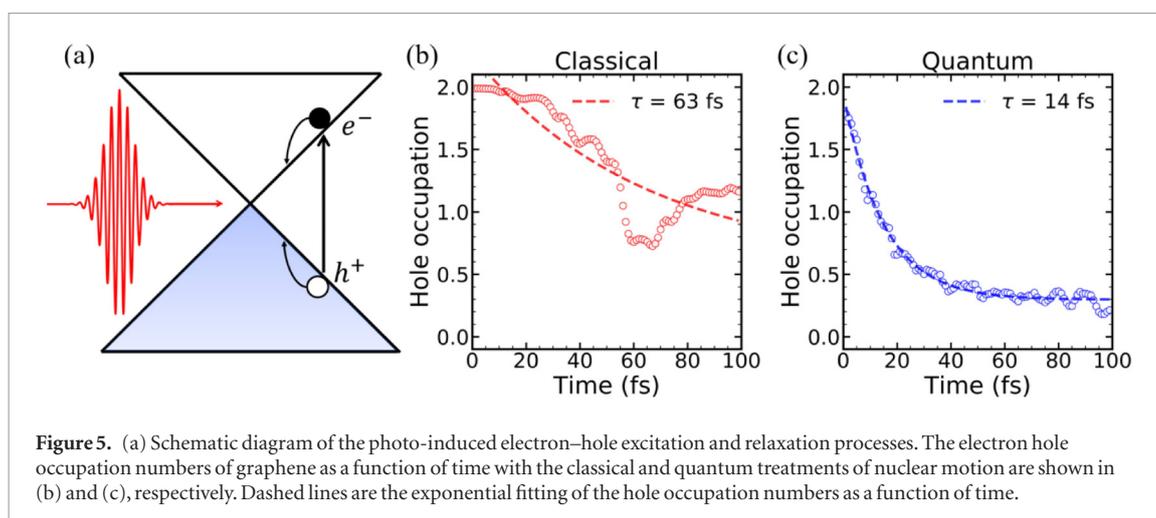
Figure 4. The radius of gyration as a function of time for photoexcited O_3 in (a) normal and (b) cyclic states at 20 K. The insets show the atomic structures of the normal (blue) and cyclic (red) forms during the RP-TDAP simulations.

We find that the excited potential energy surface plays an important role in the evolution of nuclear configurations for ozone. In response to laser stimulus, the nuclear wave packets of ozone can evolve into two distinct configurations, and the high-amount of electron excitations is the driving force for the beads to split into the normal and cyclic states. This splitting of individual beads into different branches is resulted from the different nuclei configuration in each bead, which is determined by RPMD in the time prior to splitting. In this sense, the splitting is a natural result of RPMD itself, which would be meaningful in the framework of mean field, at least to the first order. What are possibly missing in the current approach are the back reactions and correlations between excited electrons and the distribution of nuclear beads, which remains an open question. The spreading in atomic positions is influenced by the overcoherence intrinsic of the use of Ehrenfest mean-field dynamics for each bead; however, when the spreading is characterized collectively on all beads, the spreading averaged over all beads still presents a reasonable measure on the quantum distributions of atoms during the entangled electron-nuclear dynamics. We expect that with sufficient number of beads included in the simulations, this problem is alleviated since both the ground state and excited state PES are sufficiently sampled, while the ratio of problematic bead connections diminishes. We also note that the spreading of wave packet were observed in other molecules as well [42–44]. By including NQE in the rt-TDDFT calculations, specific quantum features, e.g. the splitting of quantum nuclear wave packets, can occur during the photoexcitation process, at significant variances with the averaged nuclear trajectory along the mixing potential energy surfaces in regular Ehrenfest dynamic simulations.

Graphene

We now apply the RP-TDAP approach to an extended system, the graphene crystal lattice. The ultrafast dynamics of carriers in graphene has attracted much attention [7, 45–48], because of high mobility of Dirac carriers and intriguing dynamics. Such photoexcitation dynamics and the subsequent carrier relaxation processes are governed by electron–electron and electron–phonon scatterings. Dawlaty *et al* reported an ultrafast carrier redistribution in epitaxially grown graphene layers on SiC, photogenerated by a 780 nm (1.6 eV) laser pulse. The timescale for the fast relaxation measured from time-resolved transmittivity was initially found to be in the range of 70–120 fs [7]. Recently, Rohde *et al* developed the ultrashort-time and angle resolved photoelectron spectroscopy and observed a sequence of three stages in the first 50 fs in graphene after a 1.6 eV laser photoexcitation [49]. The first

Figure 5. (a) Schematic diagram of the photo-induced electron–hole excitation and relaxation processes. The electron hole occupation numbers of graphene as a function of time with the classical and quantum treatments of nuclear motion are shown in (b) and (c), respectively. Dashed lines are the exponential fitting of the hole occupation numbers as a function of time.

stage is a photo-absorption process before 8 fs, followed by a momentum redistribution process from ~10 fs to ~22 fs, and finally a hot Fermi–Dirac distribution is reached within 50 fs.

Here we investigate quantum dynamics of charge carriers in graphene using a $4 \times 4 \times 1$ supercell containing 32 carbon atoms. We employ 12 beads for each atom during RP-TDAP simulations under the NVE ensemble. The system is first equilibrated in the NVT ensemble at 50 K for 2 ps by a ground-state RPMD simulation. Then two electrons are excited to an energy level at 3.0 eV above the Fermi level, from the level at ~3 eV below the Fermi energy. The resulting fast carrier dynamics due to electron–electron and electron–phonon scatterings is displayed in figure 5(a). With the classical treatment of the nuclei (figure 5(b)), hole occupation reduces to half of the initial value at about 60 fs. With the quantum description of nuclear motions via RP-TDAP scheme, strong quantum couplings facilitate the electron–electron and electron–phonon scatterings, and thus yield a faster carrier relaxation, compared to the classical simulation, as shown in figure 5(c). It should be noted the improved electron–electron scattering might not be straightforward to see, but it can be induced by different quantum couplings between electronic states under a range of different initial configurations. Since each bead has a different nuclear configuration from each other, this would introduce more balanced samplings of electronic occupations and couplings, yielding an improved description of electron–electron scattering. The relaxation time calculated by exponential decay fitting of hole occupation numbers obtained from quantum nuclear simulation is 14 fs, significantly shorter than that from classical simulations (63 fs). Here the hole occupation number is averaged over 12 beads. Since the initial energy of the holes (3 eV below the Fermi level) is significantly lower than that in experiment (0.8 eV below the Fermi level), the life time of the holes through carrier relaxation is expected to be about 2 times smaller than that in experiment [49]. It is clear that ultrafast charge carrier redistribution in graphene observed in experiment can be captured and well described by the quantum nuclei simulations, while classical simulations may suffer from inadequate treatment of electron–electron scatterings and electron–phonon scatterings due to the rigid ion approximation. The time evolutions of electron and hole occupation numbers in the carrier relaxation process, described in classical and quantum manners, are compared in detail in figure S4.

Conclusion

In summary, we develop a new approach, RP-TDAP, to describe the quantum motions of nuclei in electronic excited states by integrating RPMD in the rt-TDDFT framework. We derive the TDSCF equations with the external field from the TDSE with dependent evolution of nuclear coordinates and electronic wave functions. The nuclear Hamiltonian is solved using RPMD method, and the mean field forces on nuclei exerted by excited electronic states are obtained within the TDDFT evolution of Kohn–Sham orbitals. This approach can be used to study real time quantum electron-nuclei dynamics from first-principles, for both finite and periodic systems.

We perform RP-TDAP simulations on ozone molecules, as well as the infinite graphene layer, to show the quantum effects and features in the dynamics of excited states. Taking into account NQE, nuclear motion exhibits a wider distribution in atomic positions, leading to stronger orbital overlapping and enhanced charge transfer. In the photoexcitation process of ozone molecule, the nuclear wave packets split and evolve into two distinct states: the normal and cyclic configurations. The ultrafast carrier redistribution in graphene with an exponential decay behavior can be only captured in the quantum nuclear simulations, attributed to strong orbital couplings. These results indicate that NQE plays an important role in both photoexcited nuclear dynamics and carrier transport. The RP-TDAP method presented here provides a powerful simulation tool to capture and investigate the quantum state and evolution of the electrons and nuclei after photoexcitation. Further applications on

interesting quantum excitation phenomena, such as photocatalysis, non-thermal melting, and photoenhanced superconductivity are in progress.

Computational details

Ground state electronic structure is calculated using SIESTA code [50]. In RP-TDAP quantum dynamics simulations, a modified i-PI and our home-made program time-dependent *ab initio* package (TDAP) [15, 51, 52] based on SIESTA are used. The generalized gradient approximation using the Perdew–Burke–Ernzerhof functional (GGA-PBE) is chosen for the exchange and correlation energy and an energy cutoff of 200 Ry is used. For ozone, the dimension for the simulation box is $10 \times 10 \times 10 \, \text{Å}^3$. In ground-state molecule dynamics simulation, a 2 ps-long RPMD simulation with a timestep of 0.5 fs is performed in the NVT ensemble with 12 beads, and the PILE-G thermostat is employed [28, 29]. The duration for RP-TDAP quantum simulations in the constant energy ensemble is 80 fs with a timestep of 0.01 fs. For graphene, we choose a $4 \times 4 \times 1$ supercell containing 32 carbon atoms with periodic boundary conditions and a *k*-point sampling of $2 \times 2 \times 1$ in the first Brillouin zone. In 2 ps NVT simulations, the temperature is 50 K and there are 12 beads for each atom. In RP-TDAP quantum dynamics under NVE, electrons are excited into conduction band and we simulate the electron–hole relaxation process for 100 fs with a time step of 0.05 fs.

Acknowledgments

ORCID iDs

Jiyu Xu ⓘ https://orcid.org/0000-0002-2628-5492
Sheng Meng ⓘ https://orcid.org/0000-0002-1553-1432

References

[1] Ravetz B D, Pun A B, Churchill E M, Congreve D N, Rovis T and Campos L M 2019 *Nature* **565** 343
[2] Zhang M, de Respinis M and Frei H 2014 *Nat. Chem.* **6** 362
[3] Wang Q *et al* 2016 *Nat. Mater.* **15** 611
[4] Ferrari A C 2007 *Solid State Commun.* **143** 47
[5] Schaller R D, Pietryga J M, Goupalov S V, Petruska M A, Ivanov S A and Klimov V I 2005 *Phys. Rev. Lett.* **95** 196401
[6] Mehlhorn M, Gawronski H and Morgenstern K 2010 *Phys. Rev. Lett.* **104** 076101
[7] Dawlaty J M, Shivaraman S, Chandrashekhar M, Rana F and Spencer M G 2008 *Appl. Phys. Lett.* **92** 042116
[8] Deibel C, Strobel T and Dyakonov V 2010 *Adv. Mater.* **22** 4097
[9] Beck M H, Jäckle A, Worth G A and Meyer H D 2000 *Phys. Rep.* **324** 1
[10] Meyer H-D and Worth G A 2003 *Theor. Chem. Acc.* **109** 251
[11] Curchod B F E and Martinez T J 2018 *Chem. Rev.* **118** 3305
[12] Tully J C and Preston R K 1971 *J. Chem. Phys.* **55** 562
[13] Craig C F, Duncan W R and Prezhdo O V 2005 *Phys. Rev. Lett.* **95** 163001
[14] Tully J C 1998 *Faraday Discuss.* **110** 407
[15] Meng S and Kaxiras E 2008 *J. Chem. Phys.* **129** 054110
[16] Bircher M P *et al* 2017 *Struct. Dyn.* **4** 061510
[17] Meyera H D and Miller W H 1979 *J. Chem. Phys.* **70** 3214
[18] Richings G W, Polyak I, Spinlove K E, Worth G A, Burghardt I and Lasorne B 2015 *Int. Rev. Phys. Chem.* **34** 269
[19] Craig I R and Manolopoulos D E 2004 *J. Chem. Phys.* **121** 3368
[20] Markland T E and Manolopoulos D E 2008 *J. Chem. Phys.* **129** 024105
[21] Shushkov P, Li R and Tully J C 2012 *J. Chem. Phys.* **137** 22A549
[22] Wada A, Takayanagi T and Shiga M 2003 *J. Chem. Phys.* **119** 5478
[23] Yoshikawa T and Takayanagi T 2013 *Chem. Phys. Lett.* **564** 1
[24] Yoshikawa T and Takayanagi T 2014 *Int. J. Quantum Chem.* **114** 636
[25] Seki Y, Takayanagi T and Shiga M 2017 *Phys. Chem. Chem. Phys.* **19** 13798
[26] Abedi A, Maitra N T and Gross E K 2010 *Phys. Rev. Lett.* **105** 123002
[27] Agostini F, Gross E K U and Curchod B F E 2019 *Comput. Theor. Chem.* **1151** 99
[28] Ceriotti M, More J and Manolopoulos D E 2014 *Comput. Phys. Commun.* **185** 1019
[29] Kapil V *et al* 2019 *Comput. Phys. Commun.* **236** 214
[30] Andrews L and Spiker R C 1972 *J. Phys. Chem.* **76** 3208
[31] Dylewski S M, Geiser J D and Houston P L 2001 *J. Chem. Phys.* **115** 7460
[32] Matsumi Y and Kawasaki M 2003 *Chem. Rev.* **103** 4767
[33] Jones R O 1985 *J. Chem. Phys.* **82** 325
[34] Laasonen K, Car R, Lee C and Vanderbilt D 1991 *Phys. Rev. B* **43** 6796
[35] Xantheas S S, Atchity G J, Elbert S T and Ruedenberg K 1991 *J. Chem. Phys.* **94** 8054

[36] Zhu H, Qu Z W, Grebenshchikov S Y, Schinke R, Malicet J, Brion J and Daumont D 2004 *J. Chem. Phys.* **122** 024310
[37] Baloitcha E and Balint-Kurti G G 2005 *J. Chem. Phys.* **123** 014306
[38] Qu Z W, Zhu H and Schinke R 2005 *J. Chem. Phys.* **123** 204324
[39] Grein F 2009 *J. Chem. Phys.* **130** 124118
[40] Ren J, Kaxiras E and Meng S 2010 *Mol. Phys.* **108** 1829
[41] Chen J L and Hu W P 2011 *J. Am. Chem. Soc.* **133** 16045
[42] Baumert T, Engel V, Röttgermann C, Strunz W T and Gerber G 1992 *Chem. Phys. Lett.* **191** 639
[43] Averbukh I S, Vrakking M J J, Villeneuve D M and Stolow A 1996 *Phys. Rev. Lett.* **77** 3518
[44] Ergler T, Rudenko A, Feuerstein B, Zrost K, Schroter C D, Moshammer R and Ullrich J 2006 *Phys. Rev. Lett.* **97** 193001
[45] Butscher S, Milde F, Hirtschulz M, Malic E and Knorr A 2007 *Appl. Phys. Lett.* **91** 203103
[46] Lui C H, Mak K F, Shan J and Heinz T F 2010 *Phys. Rev. Lett.* **105** 127404
[47] Johannsen J C *et al* 2013 *Phys. Rev. Lett.* **111** 027403
[48] Stange A *et al* 2015 *Phys. Rev.* B **92** 184303
[49] Rohde G *et al* 2018 *Phys. Rev. Lett.* **121** 256401
[50] José M S, Emilio A, Julian D G, Alberto G, Javier J, Pablo O and Daniel S-P 2002 *J. Phys.: Condens. Matter* **14** 2745
[51] Ma W, Zhang J, Yan L, Jiao Y, Gao Y and Meng S 2016 *Comput. Mater. Sci.* **112** 478
[52] Lian C, Guan M, Hu S, Zhang J and Meng S 2018 *Adv. Theory Simul.* **1** 1800055
[53] Perdew J P, Burke K and Ernzerhof M 1996 *Phys. Rev. Lett.* **77** 3865